Parylene-Based Cuff Electrode With Integrated Microfluidics for Peripheral Nerve Recording, Stimulation, and Drug Delivery

Angelica M. Cobo, Christopher E. Larson, Kee Scholten, Jason A. Miranda, Sahar Elyahoodayan, Dong Song, *Senior Member, IEEE*, Victor Pikov, and Ellis Meng, *Fellow, IEEE*

***Abstract*— A novel Parylene C-based peripheral nerve interface that combines both electrodes and microfluidic channels in an adjustable cuff was designed, fabricated, and characterized. This minimally invasive interface incorporates a drug delivery system for targeted delivery of lysing agents and neurotrophic factors to the nerve surface to locally disrupt the epineurium and allow fascicular selectivity. Multiple platinum (Pt) electrodes were embedded in the microfluidic channels for neural stimulation and recording. The lyse-and-attract cuff electrode (LACE) uses a simple locking mechanism that is adjustable for close contact with nerves of varying diameters. Devices were fabricated using standard Parylene microfabrication techniques resulting in low variability and high device yield. A procedure for the implantation of the LACE was developed and successfully demonstrated in vivo around rat sciatic nerves. The adjustable locking mechanism demonstrated adequate holding strength and fit around the nerves. Benchtop electrochemical characterization of the thin-film Pt electrodes showed that the electrodes possessed high charge storage capacity (>1 mC/cm^2) and low impedances (<2 kΩ at 1 kHz) suitable for neural stimulation and recording. As expected, embedded electrodes demonstrated higher impedance values. Acute neural recording from the rat sciatic nerve verified the capability of the LACE to record evoked neural activity (compound action potentials). Controlled and localized microfluidic infusions were achieved at low flow rates (<1 μL/min). Finally, infusion experiments in vivo demonstrated targeted drug delivery to the sciatic nerve fascicles. This multifunctional peripheral nerve interface has the potential to enhance implant-tissue integration in vivo and provide reliable chronic performance not available in the existing extraneural or intraneural interfaces. [2018-0192]**

***Index Terms*— Cuff electrode, drug delivery, neural prostheses, microelectromechanical systems (MEMS), Parylene C, peripheral nerve.**

I. Introduction

RAPID advances in prosthetic technology, including the adoption of motorized and computerized control, offer restoration of motor and sensory functions lost to amputation, injury, or degenerative diseases. Current limb prostheses (e.g. hand, leg) provide some degree of functionality, but lack a mechanism for sensory feedback and intuitive control [2], [3]. Biological signals (e.g. electrical, mechanical, chemical) can be used to couple prostheses with the nervous system to achieve feedback control of the prosthesis [4], [5]. Interfacing the peripheral nervous system (PNS) allows other forms of sensory feedback besides visual, such as tactile and proprioceptive sensation which are necessary to provide realistic and fine motor control [6], [7]. Neural communication technologies are needed to interface with the PNS to create a fast and reliable bidirectional link between the nervous system and prostheses [4], [8]–[10] (Fig. 1). Various approaches have been developed to create stable peripheral nerve interface devices, and the most common clinically-used type consists of a cuff with electrodes placed around the nerve, enabling non-selective neural signal recording from and stimulation of the motor and afferent nerve fibers. The ideal PNS interface would provide selective stimulation of different muscle motor units, allow access to sensory afferent information, and offer mechanical compliance and biocompatible composition to reduce soft-tissue damage and foreign body reaction [11]. At the same time, designs amenable to conventional batch-scalable microfabrication would offer increased reliability and design complexity while maintaining a minimally invasive form-factor.

Existing peripheral nerve interfaces can be broadly categorized as either extraneural or intraneural/intrafasicular. Fig. 2 displays general schematics of each configuration. Extraneural interfaces record and stimulate electrical activity from outside the epineurium, the collagenous sheath encircling the nerve, whereas intraneural interfaces pierce the epineurium, achieving greater access to individual nerve fibers. The typical extraneural design, also called a nerve cuff,

Manuscript received August 13, 2018; revised October 19, 2018; accepted November 3, 2018. This work was supported in part by the Defense Advanced Research Projects Agency (DARPA) BTO under the auspices of Dr. D. Weber/Dr. E. Van Gieson through the DARPA Contracts Management Office Cooperative Agreement under Grant HR0011-15-2-0006, in part by the Viterbi School of Engineering Ph.D. Merit Fellowship (AC), and in part by the USC Provost Fellowships (CL). Subject Editor H. Jiang. *(Corresponding author: Ellis Meng.)*

A. M. Cobo, C. E. Larson, K. Scholten, S. Elyahoodayan, and D. Song are with the Biomedical Engineering Department, University of Southern California, Los Angeles, CA 90089 USA (e-mail: acobo@usc.edu; larsonce@usc.edu; kscholte@usc.edu; elyahood@usc.edu; dsong@usc.edu).

J. A. Miranda is with Galvani Bioelectronics, Stevenage SG1 2NY, U.K. (e-mail: jason.a.miranda@galvani.bio).

E. Meng is with the Biomedical Engineering and Electrical Engineering Department, University of Southern California, Los Angeles, CA 90089 USA (e-mail: ellis.meng@usc.edu).

V. Pikov is with Medipace Inc., Pasadena, CA 91101 USA (e-mail: pikov@medipaceinc.com).

Color versions of one or more of the figures in this paper are available online at http://ieeexplore.ieee.org.

Digital Object Identifier 10.1109/JMEMS.2018.2881908

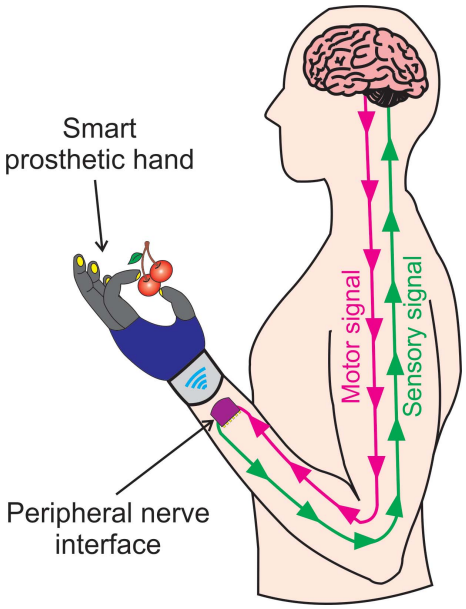

Fig. 1. Peripheral nerve interfaces necessary for brain-controlled prostheses.

consists of a flexible substrate supporting metal electrodes; nerve cuffs conformally encircle nerves, placing electrodes along the circumference of the epineurium [4], [12]–[15]. Common design features include self-sizing and locking mechanisms, which allow snug placement of electrodes on the surface of nerves of varying diameters [12], [14], [16]. Extraneural interfaces are typically defined as less invasive than intraneural interfaces, but with comparatively lower signal-to-noise ratio (SNR) during recording, and limited selectivity among different fascicles within the nerve while stimulating. Due to the low-risk of tissue damage or irritation, extraneural designs are favored for long-term (chronic, 2-11 years) applications [17], [18], but the limitations in signal fidelity and nerve selectivity preclude fine motor control required for prostheses. Improved access to individual fascicles has been achieved by extraneural interfaces which reshape the nerve, (i.e. flattening) as demonstrated by Tyler and Durand [19]. However, the SNR is still restricted by the impedance of the epineurium, and significant nerve fibers damage can be induced by the snug-fit of the interface resulting in compression and reshaping of the nerve [20], [21].

Intrafascicular/intraneural electrodes are significantly more invasive, but offer higher SNR during recordings and greater selectivity during stimulation [22], [23]. Electrodes may either be inserted longitudinally into the nerve and run parallel to nerve fibers, or transversely, and run perpendicular to fibers. Longitudinally implanted intrafascicular electrodes (LIFEs) have excellent selectivity compared to extraneural interfaces, but can only interface the nerve fibers within the targeted fascicle, and require difficult implantation surgery [24]. Transverse interfaces, such as the transverse intrafascicular multichannel electrode (TIME), can achieve single unit recordings from several nerve fibers in multiple fascicles, and can stimulate with low current requirements and high spatial selectivity [25], [26]. Transverse interfaces are associated with greater risk of nerve damage and shorter operating lifetime *in vivo*. In all cases, intraneural devices are associated with elevated physiological foreign-body response, nerve damage, tissue scarring, and, as a consequence, short operational lifetimes [27], [28]. Placement of intraneural interfaces is also difficult, due to the small size of both the recording sites (∼10-20 μm diameter) and the targeted nodes of Ranvier (∼1 μm long) [23], [27], [29], [30]. All of these challenges contribute to the very poor chronic *in vivo* performance observed with intrafascicular/intraneural interfaces. To our knowledge, chronic *in vivo* implantation of transverse and longitudinal intrafascicular interfaces has only been reported up to 2 and 6 months, respectively [24], [31]–[33].

Neither approach has achieved the desired selectivity while minimizing invasiveness, and current designs suffer from a lack of chronic reliability. To overcome these hurdles and achieve a long-term, stable interface with high fidelity recordings, we developed a minimally invasive approach in which a polymer-based, extraneural interface combines microelectronics with microfluidics to target individual fascicles within a nerve by inducing the sprouting of axonal collaterals towards electrodes embedded in microfluidic channels. This approach attempts to achieve high stability and fascicle specificity without physically damaging or penetrating the nerve. The proposed induction of collateral sprouting is based on the natural capacity of intact healthy axons to grow outside the nerve, and is applied in surgical nerve reconstruction as the end-to-side neurorrhaphy technique [34], [35]. Intact sensory and motor axons appear to have comparable capacity for collateral sprouting [36]. The sprouting can be enhanced by microsurgical removal of the connective sheaths (epineurial and perineurial layers) of the nerve [37]–[39]. In contrast to the microsurgical removal of epineurium and perineurium, we propose an enzymatic removal of collagen fibers to avoid the risk of a nerve injury [40]. Application of exogenous factors such as neurotrophic factors (e.g. nerve growth factor (NGF) and methylcobalamin) can significantly improve collateral sprouting from an intact nerve [41]–[43]. Neurotrophic factors for collateral sprouting are commonly delivered via frequent intraperitoneal or epineurial injections, or silicone reservoir chambers [41], [43]–[45]. Injections result in additional mechanical injury and risk of infection, while reservoir chambers have a limited drug payload. Improved delivery of exogeneous factors can be achieved via implantable microfabricated microfluidics to allow for chronic, localized, and aseptic delivery.

Our peripheral nerve interface approach aims to selectively induce axonal sprouting from the nerve fascicles via localized delivery of lysing agents to temporarily disrupt the epineurium, followed by delivery of neurotrophic factors to promote axonal sprouting towards electrodes within the microchannels. The design comprises a thin-film polymer 'cuff' with adjustable diameter to ensure localized diffusion of chemicals into the epineurium of nerves of varying diameters. This Lyse-and-Attract Cuff Electrode (LACE) aims to increase fascicular selectivity and signal-to-noise ratio for recording and/or stimulation without traumatic invasiveness, while providing long-term stability beyond the current state of the art. Preliminary characterization of the LACE was presented in prior studies [1], [46]. This study presents details

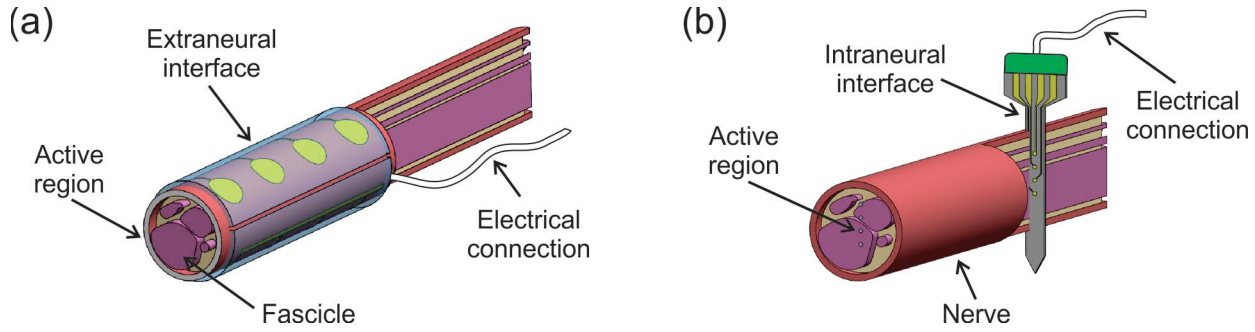

Fig. 2. (a) Extraneural interfaces wrap around the nerve and record/stimulate from the nerve surface. (b) Intraneural interfaces penetrate the nerve gaining greater access to individual nerve fibers.

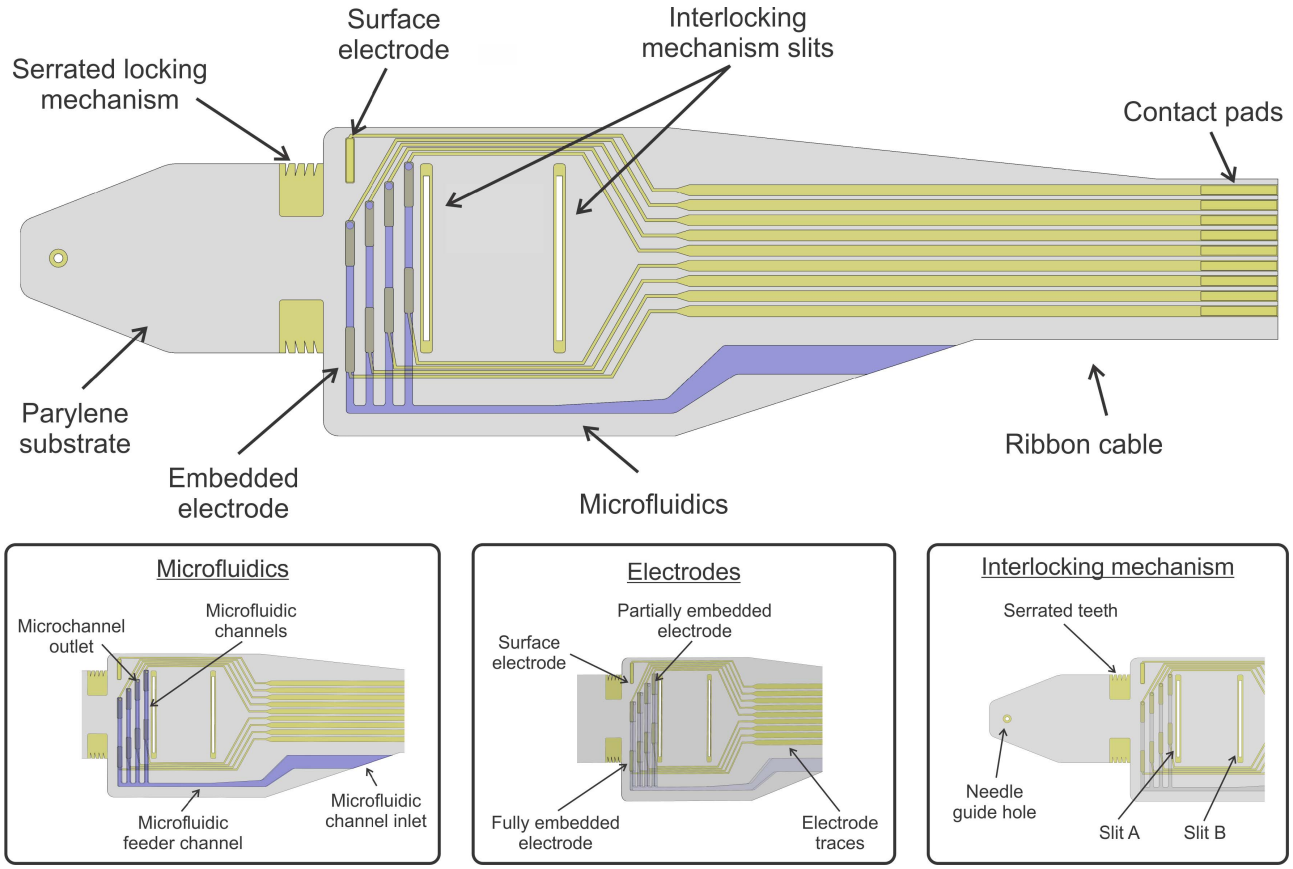

Fig. 3. Illustration of LACE device with major components labeled.

on the design and fabrication of this novel peripheral nerve interface. This study also presents the characterization of the mechanical interlocking mechanism, drug delivery, and electrical recording and stimulation functionalities of the device as well as initial *in vivo* implantation, and acute neural recording and drug delivery results.

II. Design

The LACE is a multifunctional device that combines drug delivery, electrical recording and/or stimulation, and a mechanical interlocking mechanism. The LACE is fabricated from thin-film Parylene C. Parylene C is a USP class VI biocompatible polymer, chemically inert, and has a low Young's modulus (~2-3 GPa) to more closely match the mechanical properties of the biological tissue [47], [48]. In addition, the high dielectric strength of Parylene C provides excellent electric insulation for isolation of recording/stimulating channels. The LACE incorporates four surface micromachined microfluidic channels for drug delivery with each microfluidic channel containing a pair of Pt electrodes for differential recording and/or stimulation (Fig. 3). The cuff encircles the nerve with the microfluidic outlets in direct contact with the circumference of the epineurium, and is held in position by the serrations of the interlocking mechanism. Ancillary components identified in Fig. 3 include the channel inlet for external fluidic connection, Parylene ribbon cable for external electrical connection,

and a reference electrode external to the microfluidic channels. The LACE functionalities are described below in greater detail.

A. Microfluidic Channels

The LACE incorporates four surface micromachined Parylene C fluidic channels with a wall thickness of 8 μm (250 μm W $\times$ 20 μm H). The microfluidic channels are designed for targeting multiple fascicles in a rat sciatic nerve: sural, tibial, peroneal, and cutaneous [49]. The channels will deliver lysing agents followed by neurotrophic factors to the encircled peripheral nerve (PN). Microfluidic channel outlet ports are greater than 100 μm in diameter to encourage active and vascularized axons to grow into the microfluidic channel for high SNR recording. The outlet ports are staggered to reduce diffusion/interaction between different channels. A microfluidic channel branch design was chosen to ensure equal pressure drop, and hence flow rate, across all channels (Fig. 3). Previous fluidic channel characterization in the curl configuration demonstrated fluid flow blockage through the distal fluidic channel [1], [46]. Channel collapse was observed along the horizontal channel and can be attributed to the strong stiction forces between the top and bottom Parylene layers of the microfluidic channels. In this study, the fluidic channels incorporate polymer support walls (20 μm W $\times$ 20 μm H $\times$ 390 μm L) along the horizontal channel to improve mechanical robustness, particularly during deformation as if encircling a nerve and allow flow through all channels [50], [51]. Mid-channel support walls are fabricated from Parylene along the horizontal feeder channel to prevent channel collapse after encircling a nerve. External fluidic connection to the device is established at the microfluidic channel inlet.

B. Electrodes

The LACE features eight platinum (Pt) electrodes (300 μm W $\times$ 1500 μm L) for differential recording and stimulation, with a pair of corresponding electrodes located in each of the four microfluidic channels, spaced 3 - 4 mm apart. The electrodes are thin-film (200 nm thick) and lithographically patterned on the Parylene C base which comprises the LACE body. The electrodes are rectangular, with rounded edges, to avoid high current density at sharp edges [52]. The dimensions were chosen to fit within the constrained real estate of the microfluidic channels, while providing a low electrochemical impedance range of 2 – 5 kΩ at 1 kHz (surface area of approximately 0.45 mm^2) [53]–[55]. Pt was selected as the electrode material due to high resistance to corrosion in *in vivo* environments, low decomposition characteristics during stimulation, and high charge injection limit [56]–[58]. A surface electrode, outside the microfluidic channel, serves as a reference, while an unintegrated Pt wire provides a connection to ground. Electrical connections to each electrode are likewise thin-film Pt leads, lithographically patterned, which span the length of a Parylene ribbon cable (~2 cm long), terminating in a series of nine individual contact pads for external electrical connection.

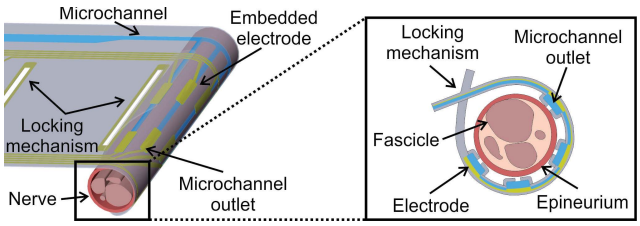

Fig. 4. Schematic of LACE for targeting individual fascicles within a nerve. Inset shows the cross-sectional view.

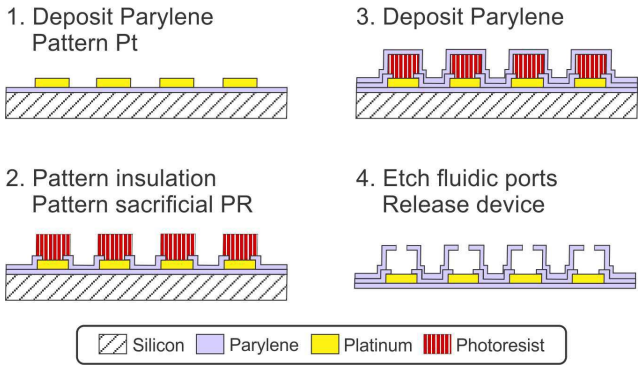

Fig. 5. Simplified LACE fabrication process which utilizes standard surface micromachining techniques for Parylene.

C. Interlocking Mechanism

The cuff incorporates an adjustable interlocking mechanism which allows the device to securely fasten around nerves of varying diameters, keeping the microfluidic ports in direct contact with the epineurium for highly localized drug delivery. The interlocking mechanism consists of an elongated tapered tab that loops around the sciatic nerve with the microfluidic outlets in direct contact with the circumference of the epineurium, inserts into the etched slit A, and is held in position by etched, metal-reinforced serrations (Fig. 3 and Fig. 4). A two-part locking mechanism is used to maintain the loop around the nerve, and includes slit B through which the tab is threaded to achieve a secure buckle lock. A micromachined hole in the tab can be used to pass a needle with suture, and facilitate guiding of the tab through the slits resulting in the suture locking technique. The cuff is adjustable (1.1-1.5 mm diameter, 0.1 mm increments) to provide close fit to nerves of varying diameter. Device dimensions were chosen to fit the sciatic nerve of a 340 g adult male rat with an average sciatic nerve diameter ranging from 1.2 to 1.4 mm. The horizontal diameter of the sciatic nerve increases at the fascicle separation zone, but the nerve also flattens resulting in a consistent total circumference. 12 mm length of the sciatic nerve can be easily exposed to allow the insertion and placement of a cuff up to 10 mm in length.

III. Fabrication

Devices were fabricated on a bare silicon (Si) wafer, which provided mechanical support during the microfabrication process (Fig. 5). A 10 μm Parylene base layer (Parylene C, Specialty Coating Systems, Indianapolis, IN) was first deposited by chemical vapor deposition onto a dehydrated (baked at 110 °C, > 20 min) Si wafer. Sputtered Pt electrodes, leads, and contact pads (2000 Å, LGA Thin Films,

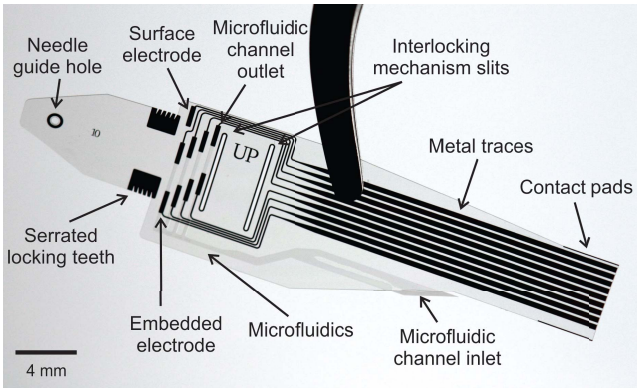

Fig. 6. Fabricated LACE.

Santa Clara, CA) were then patterned by a liftoff process using a negative photoresist mask (AZ 5214 E-IR; Integrated Micro Materials, Argyle, TX). A 10 μm Parylene insulation layer was then deposited and selectively etched with oxygen plasma to expose electrodes and contact pads. A photoresist layer (AZ 4620; Integrated Micro Materials, Argyle, TX) was spun to a thickness of 20 μm, and patterned to form the sacrificial structures defining the microfluidic channels. An 8 μm Parylene layer was then deposited over the sacrificial photoresist to create the microchannels. Oxygen plasma etching (700 W ICP, 20 W RF, 23 mTorr) was used to expose the surface electrode and contact pads, create openings for microfluidic ports, and micromachine the LACE outline. Devices were released from the substrate while submerged in DI water (Fig. 6). The long ($\sim$27 mm length) sacrificial layer of photoresist, which defined the microfluidic channel interior, was removed by soaking devices in a warm (40 °C) and agitated (170 rpm magnetic stir-bar) acetone bath. No stiction of Parylene structures was observed. A steel microwire (200 μm OD) was inserted into the fluidic channel inlet prior to thermal annealing, in order to thermoform the Parylene channel inlet to the desired shape and width. LACE devices were annealed under vacuum at 200 °C for 48 hours, followed by a slow cooling step to room temperature (>12 hrs) also under vacuum [59].

Fluidic connection to the LACE consisted of a custom-made polyurethane (PU) catheter (SAI Infusion Technologies, Lake Villa, IL). The PU catheter was inserted into the thermoformed microfluidic channel inlet and secured in place with Loctite 4902 (Loctite, Westlake, OH) and MED-4210 silicone (Factor II, Inc., Lakeside, AZ) medical grade epoxies. External electrical connection was established using a zero-insertion force connector (ZIF, part no. 0514411072 Molex Inc.) and flat flexible cable (FFC, part no. 050R10-102B, Parlex, Methuen, MA) connection. The LACE contact pad region was stiffened with polyetheretherketone (PEEK) polymer tape with silicone adhesive (37-5S 5 and 37-2S 2, CS Hyde Company, Lake Villa, IL) to match the required cable thickness for the ZIF connector.

IV. Experimental Methods

A. Mechanical Evaluation

The metal reinforced interlocking mechanism was tested by wrapping and unwrapping LACE devices around agarose nerve phantoms and evaluating holding strength under gentle handling conditions (Fig. 7, Fig. 8, n > 4). An agarose concentration of 1.37 % wt/wt in water was selected to produce a 'phantom' nerve from agarose gel with a compressive modulus comparable to that of rabbit sciatic nerve [46], [60], [61]. Agarose nerve phantoms were fabricated with diameter of 1.3 mm, which falls within the measured sciatic nerve diameter range for a 340 g adult male rat.

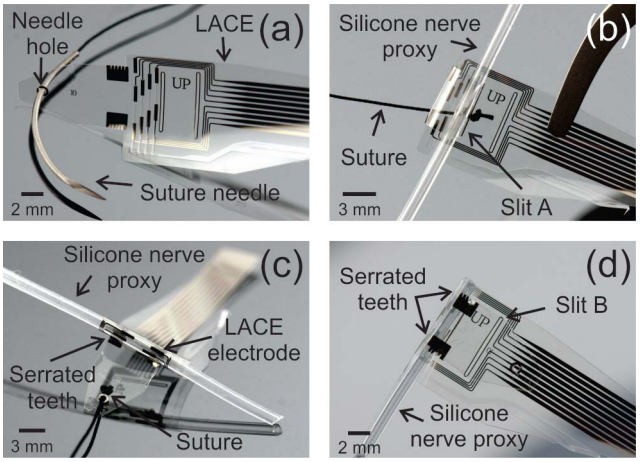

Fig. 7. Micrographs of the LACE adjustable interlocking mechanism and the suture locking technique previously described. (a) Suture needle passed through the needle hole, (b-c) tab threaded through slit A and kept in place by serrated teeth, and (d) tab secured by threading through slit B to form the buckle locked structure.

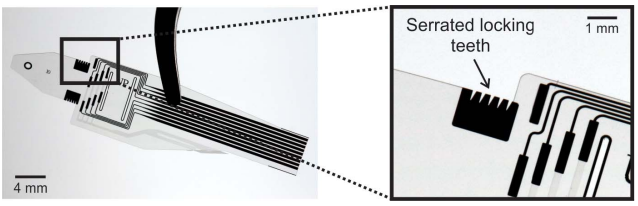

Fig. 8. Micrographs of the LACE interlocking mechanism serrated teeth.

The interlocking mechanism was tested *in vivo* by wrapping LACE devices around the sciatic nerve of anesthetized rats, and assessing its holding strength under handling conditions expected during implantation. All procedures for the animal experiments were in accordance with the animal protocols approved by the United Kingdom Home Office, the Animal Care and Use Review Office (ACURO) of the US Army Medical Research and Material Command, and the Institutional Animal Care and Use Committee (IACUC) and the Department of Animal Resources of the University of Southern California (DAR, USC). Adult male rats weighing between 400-450 g were used in this study. Animals were anesthetized with isoflurane. The left dorsal hind limb was shaved from the ankle to the midline, about 1 cm rostral to the femur. A 1.5 cm incision was made at the thigh directly over the femur and the sciatic nerve was exposed. The LACE device was surgically placed around the sciatic nerve as shown in Fig. 9. The tab of the LACE device was fed under the nerve with the fluidic channel outlet ports in contact with the nerve. The tab was then threaded through slit A and secured in place at the appropriate serrated tooth, making sure the device fit securely

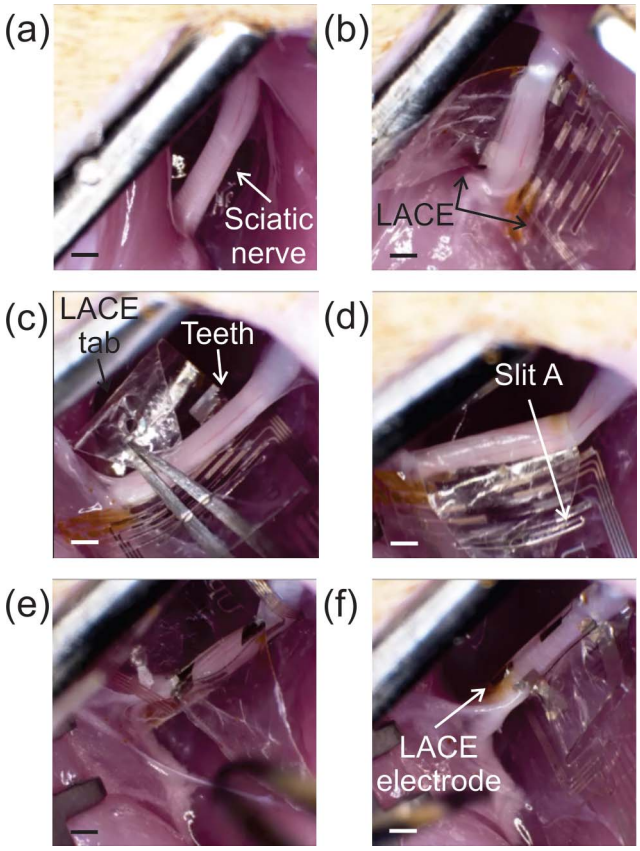

Fig. 9. Sequence of photographs illustrating the *in vivo* implantation of the LACE around the sciatic nerve of an anesthetized rat. (a) Exposed sciatic nerve, (b) device fed under the nerve with fluidic ports in contact with the nerve, (c-d) tab threaded through slit A, (e) tab kept in place by serrated teeth, and (f) LACE securely wrapped around the sciatic nerve. Scale bar is 1 mm.

around the nerve. Devices were handled with surgical forceps during *in vivo* implantation as opposed to the suture locking technique.

B. Electrical Evaluation

Cyclic voltammetry (CV) and electrochemical impedance spectroscopy (EIS) were used to assess the stimulating and recording capabilities of the cuff electrodes in initial benchtop testing. Measurements were performed on LACE devices without microfluidic channels (surface electrodes) in both flat and curled configurations, as well as on electrodes embedded in the microfluidic channels. All measurements were performed with a Gamry Reference 600 potentiostat (Gamry Instruments, Warminster, PA). CV was performed in a solution of 0.05 M H_2SO_4 to electrochemically clean the electrode surfaces. The stimulation characteristics of the electrodes were subsequently assessed with CV measurements in a solution of phosphate buffer saline (1× PBS). Both measurements were performed under a constant stream of N_2 using a three-electrode cell. The working electrode was cycled between −0.2 to 1.2 V for 0.05 M H_2SO_4 or −0.6 to 0.8 V for 1× PBS, with respect to a Ag/AgCl (3M NaCl) reference, a potential range that is within the water window [46], [62], [63]. A 1 cm^2 Pt plate served as a counter electrode. Full voltammetric sweeps were repeated

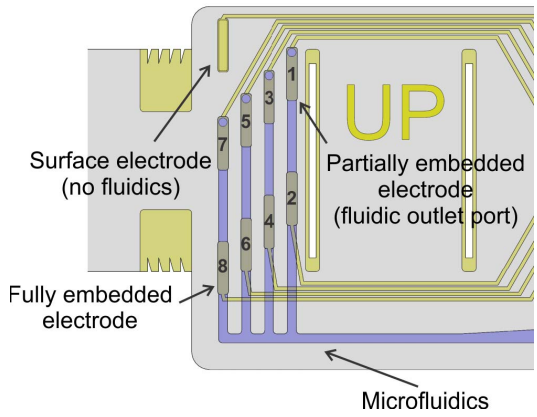

Fig. 10. Diagram of LACE with fluidic channels showing detailed electrode layout.

for 30 cycles at a scan rate of 250 mV/s. EIS was performed in 1× PBS at room temperature with an AC perturbation signal of 25 mV (rms) in the frequency range of 1-10^5 Hz. As with CV, a Ag/AgCl (3M NaCl) reference and 1 cm^2 Pt plate counter were used.

In vivo recording of compound action potentials (CAPs) of a rat sciatic nerve was performed in acute experiments. Anesthesia was induced in a male Wistar rat 6 weeks of age, weighing 300 g, with an injection of ketamine and xylazine combination. Two hours after the anesthetic injection, an inhaled mixture of oxygen and isoflurane was delivered to prolong the anesthetic effect for the remainder of the procedure. To confirm proper anesthetic level, toe pinch withdrawal reflexes were tested throughout the surgery. The right thigh was shaved and a midsagittal incision was made. Muscles were exposed and blunt-dissected. The sciatic nerve was then exposed and rinsed using PBS. The LACE was then secured around the sciatic nerve using the suture locking technique. The LACE surface electrode and electrode 7 (Fig. 10) were connected differentially to the recording amplifier at 80 dB gain. A large platinum ground electrode was attached to the animal's exposed muscle near the incision site. Signals were sampled at 100 kHz through a 10 Hz - 10 kHz band pass filter using a multi-channel recording system (Digidata 1322A, Molecular Devices, Sunnyvale, CA) and pClamp9 software. CAPs were evoked by bipolar monophasic current pulses (200 μs duration, 150 μA amplitude) delivered through a pair of needle electrodes inserted into the nerve 2 cm proximal to the LACE. The resulting neural activity was recorded using the LACE. The recording procedure was repeated after nerve conduction blockage with the application of lidocaine to the nerve to confirm the neural source of the previously recorded signal [64].

C. Microfluidic Evaluation

The fluidic integrity of microchannels in flat and curled LACE devices was evaluated by driving a colored dye through the channels using an infusion pump (Infuse/Withdraw PHD 2000, Harvard Apparatus, Holliston, MA) and imaging the progression of the dye with a calibrated microscope (HD60T, Caltex Scientific, Irvine, CA). LACE devices were

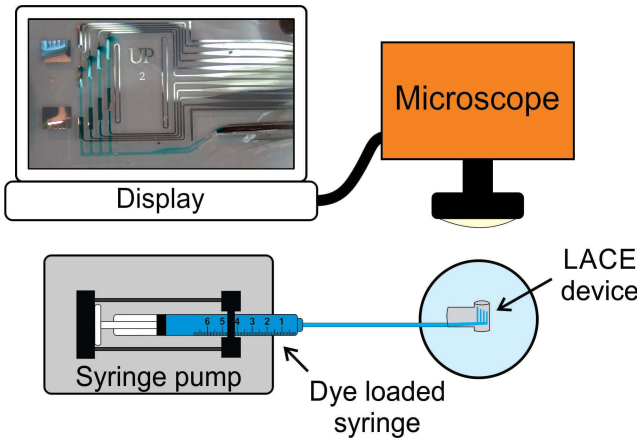

Fig. 11. Microfluidics evaluation experimental setup.

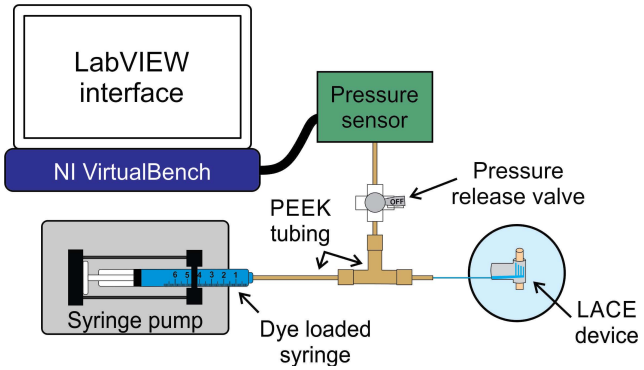

Fig. 12. Schematic diagram of experimental setup to determine bursting pressure of microfluidic channels.

primed to remove any trapped bubbles in the channels by flushing the channels with isopropyl alcohol and distilled water for 5 minutes each, while the device was submerged in a bath of either solution. A schematic of the testing setup is depicted in Fig. 11. Microchannels in flat devices were tested with flow rates ranging from 5 nL/min to 2000 nL/min. This range was selected based on the typical epineurial space drug delivery rate of 17 nL/min [46], [65]. Flow through each channel was also evaluated in curled devices [1]. Curled devices were placed upright in an acrylic jig and infused with a color dye at a flow rate of 500 nL/min while imaging the transverse progression of the dye as previously described. The fluidic channel inlet connection on another set of LACE devices was tested with flow rates starting at 800 nL/min at increments of 200 nL/min with 1 minute of test duration at each flow rate. Any visible leaks or Parylene layers delamination around the fluidic channels or connection were considered as failure.

Pressure at which the device microfluidic channels fail (e.g. leaks, delamination) was determined empirically. Pressure measurements were collected at various flow rates using a pressure sensor (ASDX001D44R, Honeywell International Inc., Morristown, NJ) powered by a NI VirtualBench (VB-8012, National Instruments Corp., Austin, TX) as shown in Fig. 12. The LACE device was wrapped around an agarose nerve phantom and colored dye was infused through the channels at a flow rate of 900 nL/min while monitoring for channel failure. Pressure sensor data was read by a data acquisition unit (LabVIEW 15.0 with NI VirtualBench VB-8012).

Localization of fluid delivery was demonstrated by encircling a LACE around a sciatic nerve phantom and driving a color dye through the microfluidic channels [1]. The nerve phantom was produced from a molded polydimethylsiloxane (PDMS) core covered with an absorbent wood fiber wipe (Kimtech Science Kimwipe, Kimberly-Clark, Irving, TX). The nerve phantom was selected to mimic the size of a 340 g adult male rat sciatic nerve and to facilitate fluid delivery visualization during infusion studies. LACE devices were primed as previously described and then locked around the nerve phantom. Dye was infused using an external syringe pump at 100 nL/min flow rate until it reached the fluidic outlet ports. The nerve phantom was imaged using an optical microscope to help visualize the degree of localization.

A series of acute *in vivo* infusion experiments were performed to determine the optimal infusion regimen through the LACE microfluidic channels to achieve localized drug delivery on the rat sciatic nerve. These experiments are necessary to determine the correct flow rate for delivering the lysing agent in future chronic experiments. Methylene blue dye, commonly used for staining peripheral nerve tissue [66], was used to help visualize localized fluid diffusion into the nerve. The LACE microfluidic channels were primed *ex vivo* as previously described. The dye was infused *ex vivo* until it reached the LACE microfluidic channels. During priming, air bubbles became trapped within some of the microfluidic channels resulting in temporary flow obstruction. Devices with at least three functioning microfluidic channels were selected for *in vivo* infusion experiments.

Devices primed with the dye were surgically placed around the sciatic nerve of anesthetized rats as described above. With the LACE tight around the nerve, dye was infused at various flow rates (17 to 250 nL/min) and durations (5 min to 4 hours). Following dye infusion experiments, the animals were sacrificed and the nerves dissected. The nerves were imaged for evidence of dye diffusion on the surface and penetration into the nerve via optical micrographs and histology, respectively. 10 to 15 μm sections were cut with a cryostat for histology evaluation.

V. Experimental Results

A. Mechanical Evaluation

The interlocking mechanism was simple to implement and robust. The suture locking technique facilitated wrapping the device around the agarose nerve phantom. The LACE devices wrapped tightly around the phantoms and did not disengage during fluidic testing, evidence of a secure lock. No damage to the agarose nerve phantom or the cuff was observed despite repeatedly engaging and releasing the lock and curling and uncurling the LACE devices around the nerve phantom. LACE devices were safely and securely implanted around the sciatic nerve of male rats. The interlocking mechanism allowed LACE devices to wrap tightly around the rat sciatic nerve without sliding of the device. No damage to the rat sciatic nerve was observed when engaging and releasing the lock or during *in vivo* infusion experiments. However, cuff damage was

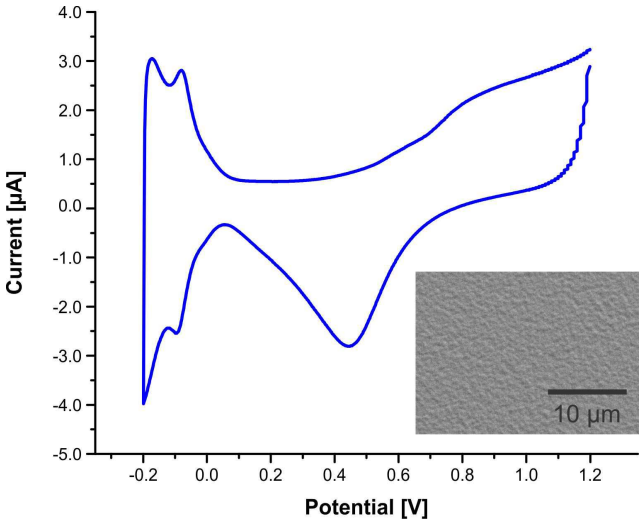

Fig. 13. Representative cyclic voltammetry in H_2SO_4 of a single recording site without microfluidic channels yielded standard Pt electrode characteristics. Inset shows SEM micrograph of representative Pt electrode with characteristic roughness.

observed during some implantation surgeries due to rough handling with surgical tweezers.

B. Electrode Evaluation

Fig. 13 displays a representative voltammogram of an electrode in sulfuric acid, sans microfluidic channel. The electroactive surface area (ESA) calculated from the CV data was 688,810 ± 67,116 μm^2 (n=4), which is higher that the geometric surface area (GSA) of 475,396 μm^2 due to surface topology. Stimulation electrodes can be characterized by their cathodal charge storage capacity (CSC) [46], [63]. The cathodal CSC in 0.05 M H_2SO_4 and 1× PBS were not significantly different as confirmed by statistical analysis (ANOVA, $p > 0.05$) with a calculated value of 1.64 ± 0.4 mC/cm^2 and 1.09 ± 0.1 mC/cm^2, respectively. No bubble generation was observed during the CV, indicating operation within the water window which is important for safe electrical stimulation.

Surface electrodes had an impedance of 1.8 ± 0.11 kΩ and a phase of −56.4 ± 1.0° at 1 kHz, with little variation between electrodes (n = 6) [46]. Minimal variation in impedance was observed following curling or other deformation of the polymer cuff; Fig. 14 and Table 1 present the impedance magnitude and phase at 1 kHz for electrodes prior to curling the LACE, while curled, and uncurled. As expected, electrodes embedded in a microfluidic channel exhibited different CV curves and higher impedance values, which are attributed to increased solution resistance, due to the longer resistive pathway imposed by the length of the microfluidic channel (Fig. 10, Fig. 15, Fig. 16, and Table 2). This is supported by the observed decrease in current output in the CV curves and the increase in impedance for the electrodes embedded deeper within channels.

The evoked CAP, comprised of a summation of action potentials in multiple A fibers, was successfully recorded using

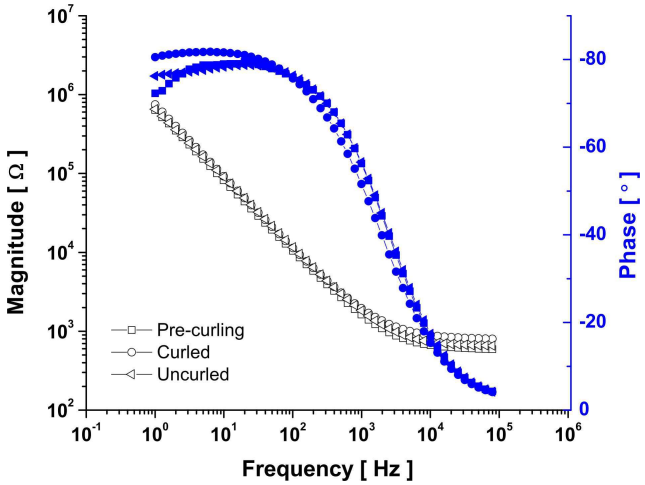

Fig. 14. Electrochemical impedance spectroscopy plot of a LACE device in pre-curling, curled, and uncurled configuration (mean ± SE, n = 3 electrodes).

TABLE I
ELECTROCHEMICAL IMPEDANCE SPECTROSCOPY IN 1× PBS AT 1 kHz (MEAN ± SE, N = 3) OF SURFACE ELECTRODES IN A LACE DEVICE IN PRE-CURLING, CURLED, AND UNCURLED CONFIGURATION

Device configuration	*Impedance magnitude (kΩ)*	*Impedance phase (°)*
Pre-curling	1.61 ± 0.1	-54.70 ± 1.4
Curled	1.99 ± 0.1	-49.60 ± 1.0
Uncurled	1.70 ± 0.1	-53.93 ± 1.4

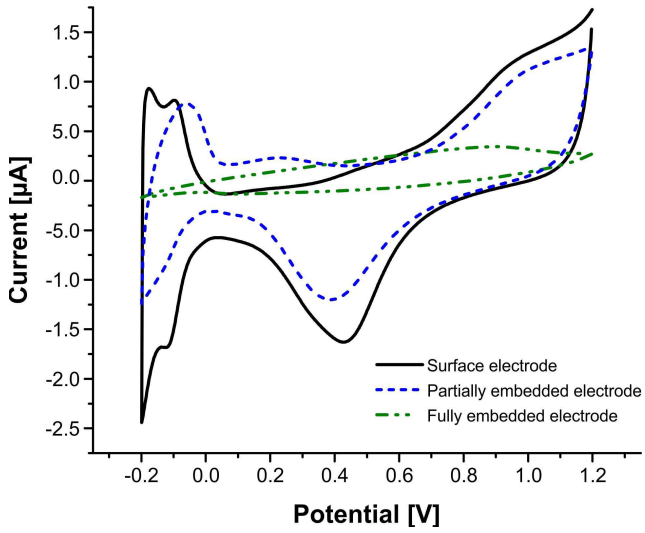

Fig. 15. Representative cyclic voltammogram of LACE Pt electrodes in sulfuric acid following priming.

the LACE as shown in Fig. 17. Recordings after lidocaine application to the sciatic nerve showed only the stimulus artifact.

C. Microfluidic Evaluation

Uniform flow through all microfluidic channels and outlet ports was observed with devices in the flat configuration

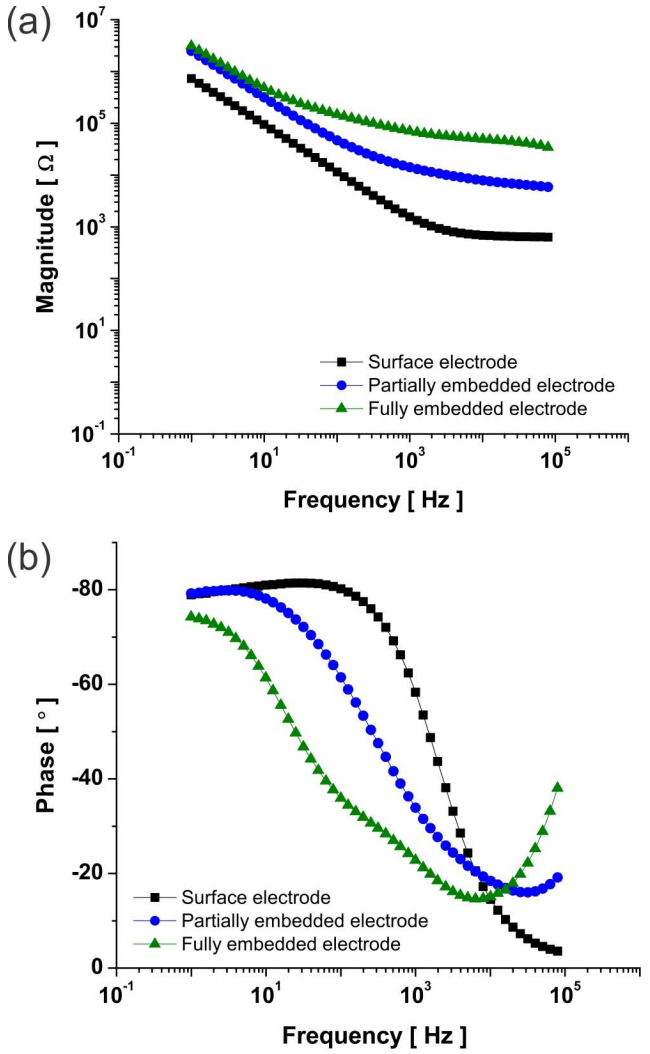

Fig. 16. Representative electrochemical impedance spectroscopy plots of impedance (a) magnitude and (b) phase in 1×PBS for a surface electrode with no fluidics, partially embedded electrode (fluidic outlet port), and fully embedded electrode.

TABLE II
ELECTROCHEMICAL IMPEDANCE SPECTROSCOPY IN 1× PBS AT 1 kHz (MEAN ± SE). PARTIALLY EMBEDDED ELECTRODES ARE LOCATED UNDERNEATH THE FLUIDIC OUTLET PORT

Electrode state	***n***	***Impedance magnitude (kΩ)***	***Impedance phase (°)***
No fluidics	4	2.99 ± 0.22	-59.39 ± 3.92
Partially embedded	12	13.57 ± 2.11	-35.07 ± 3.14
Fully embedded	11	48.11 ± 6.98	-21.40 ± 4.52

(Fig. 18, n=8). No leakage or Parylene delamination was observed up to a flow rate of 2000 nL/min. Flow through all fluidic channels and outlet ports was also achieved in cuff devices in the curled configuration (n = 3) (Fig. 19). The fluidic connection was flexible and robust with no failure

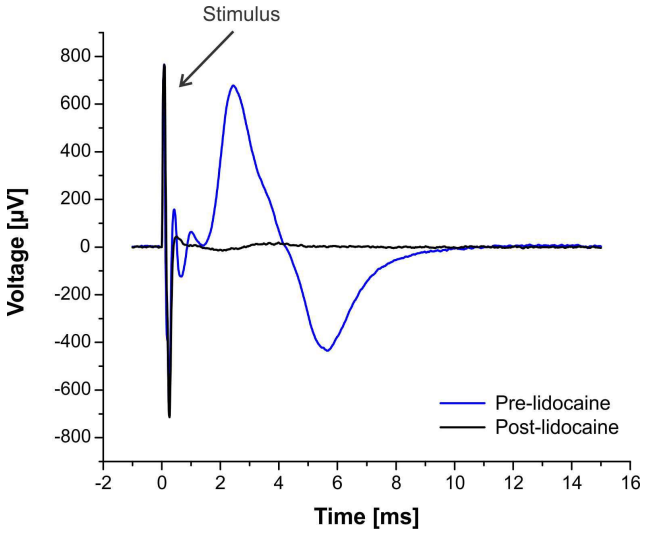

Fig. 17. Evoked compound action potential followed by evoked putative electromyographic (EMG) response from the leg muscles, recorded in a rat sciatic nerve by the LACE. Recordings after lidocaine application to the sciatic nerve showed only the stimulus artifact.

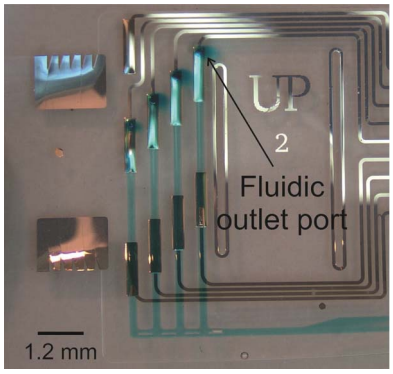

Fig. 18. Representative optical micrograph of the infusion experiment at 500 nL/min flow rate while the device was in the flat configuration.

observed up to a flow rate of 2500 nL/min (n=5). The mean pressure at which device failure occurred was 0.39 ± 0.07 psi (2.69 ± 0.48 kPa, n=3).

Localized delivery on nerve phantoms was confirmed as shown in Fig. 20. Differing flow rates among individual channels resulted in slightly different diffusion area. Flow was achieved through at least three microfluidic channels which is sufficient for the *in vivo* application. Minimal transverse and longitudinal dye diffusion observed in this study demonstrates the potential for highly localized *in vivo* delivery of lysing agents and neurotrophic growth factors.

LACE devices successfully infused rat sciatic nerves. After implantation, some non-functioning fluidic channels became functional while in some cases only 1 to 2 ports remained functional, which might indicate displacement of air bubbles or device damage during implantation, respectively. A slow flow rate (17 nL/min) for a prolonged duration (4 hrs) provided localized dye diffusion regions on the epineurial surface of the nerve as shown in Fig. 21a; however, the histology showed no evidence of dye penetration into

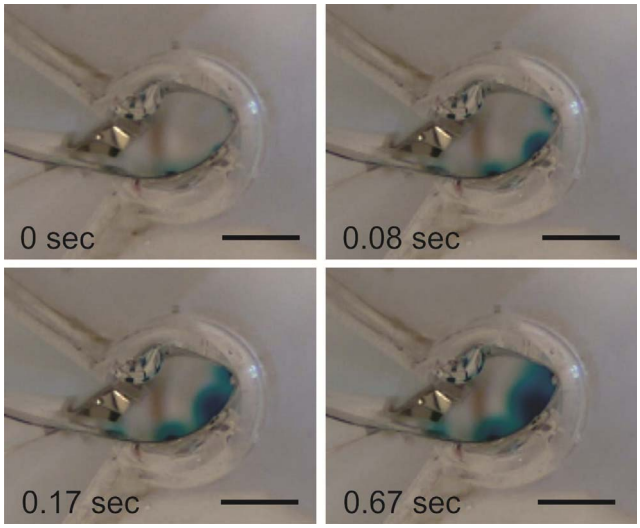

Fig. 19. Representative sequential optical micrographs of the infusion experiment in a curled device at 500 nL/min flow rate (transverse view). The channels were primed with the dye introduced at the microfluidic channel inlet. Scale bar is 1 mm.

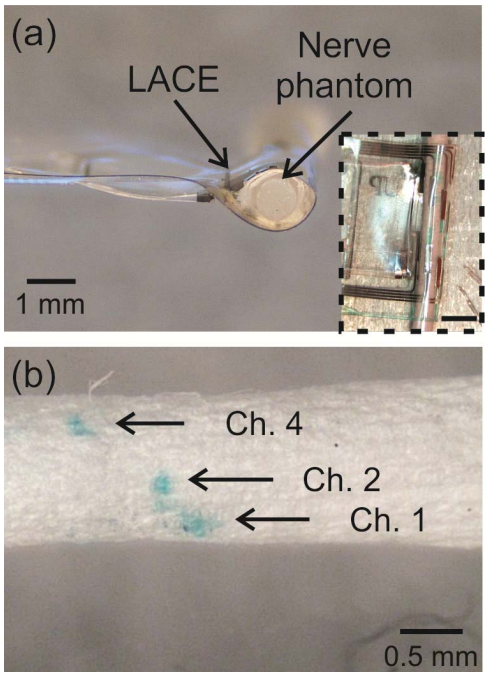

Fig. 20. (a) Transverse view of LACE wrapped around a nerve phantom. Inset shows side-view. (b) Representative nerve phantom after localized dye delivery (n = 3). Inset scale bar is 2 mm (reprinted with permission from [1] ©2017 IEEE).

the nerve fascicles. Given that the lysing agent will disrupt the connective tissue, such a flow rate may lead the solution to penetrate the nerve and result in highly localized axonal sprouting (Fig. 21b). A flow rate between 50 – 67 nL/min for more than 2 hours resulted in non-localized coverage of the nerve circumference, with non-localized dye penetration into the nerve. A faster infusion rate (250 nL/min) for a shorter time (5 minutes) showed non-localized coverage of the nerve surface with localized dye diffusion into the smallest fascicles of the nerve as shown in Fig. 22.

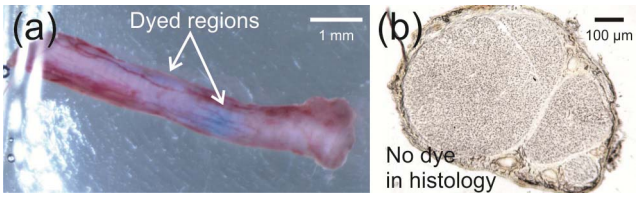

Fig. 21. (a) Localized dye delivery shown as two discrete spots of dye from two different microchannel outlet ports on the surface of the nerve with a flow rate of 17 nL/min for 4 hours. (b) Histology showed no dye diffusion into the nerve.

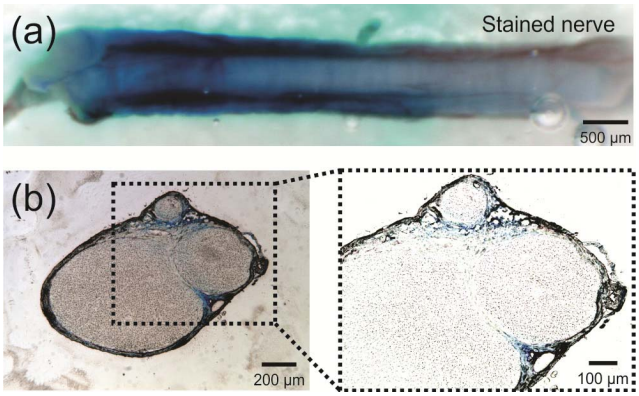

Fig. 22. (a) Sciatic nerve infused with a 250 nL/min flow rate for 5 minutes showed non-localized dye coverage of the nerve. (b) Histology results showed dye penetration into the smallest fascicles.

VI. Discussion

The adjustable interlocking mechanism was simple to implement and provided a secured hold around nerve phantoms and rat sciatic nerves. No damage was observed during repeated engaging and disengaging of the cuff which allowed readjustment of the device around the nerve during implantation resulting in adequate fit. The LACE adjustable interlocking mechanism allowed for a secured and tight fit around the sciatic nerve while minimizing mechanical damage to the delicate nerve tissue commonly seem in cuff interfaces surgically secured by suturing to the epineurium [4], [12], [46]. Additionally, this microfabricated thin-film locking mechanism avoids the use of bulky handmade external fixation components and complex assembly [14], [46].

Electrochemical (EC) techniques were utilized to assess the recording and stimulation capabilities of the electrodes. CV on LACE electrodes without microfluidic channels (surface electrode) demonstrated high CSC (>1 mC/cm^2) values suitable for stimulation of neural tissue. CV proved to be a useful EC technique for cleaning of the electrode surface, and determining true ESA and CSC. EIS of LACE surface electrodes in flat and curled configuration demonstrated low electrical impedance ($\sim$2 kΩ) values at 1 kHz suitable for peripheral nerve recordings. Minimal variation in impedance magnitude and phase at 1 kHz with curling of the device indicated that curling does not affect electrode performance. Recorded impedances are expected to help reduce susceptibility to noise pickup from sources such as muscle outside the cuff or recording equipment [14], [46] to provide adequate neural recording

potential. High impedance values of embedded electrodes are attributed to increased solution resistance, due to the longer resistive pathway imposed by the length of the microfluidic channel. For the electrodes embedded within the microfluidic channel, the current must travel through the relatively narrow channel to the counter electrode as oppose to traveling through the bulk solution resulting in higher impedance. This was exhibited in EIS with a larger impedance magnitude at higher frequencies compared to an electrode not embedded in a microfluidic channel (Fig. 16a). As these electrodes are intended to be used on axons that have grown into the microchannels, the increased impedance is not expected to adversely affect recordings. Instead, the close proximity of a specific axon to the recording site is expected to improve nerve selectivity and signal fidelity. The choice of electrode material, dimensions, and design resulted in cuff electrodes with suitable electrode properties for peripheral nerve recording and stimulation. The LACE successfully recorded evoked A-fiber CAPs from a rat sciatic nerve during acute *in vivo* recordings. Additional acute recordings with lidocaine application to the sciatic nerve, which blocks the action potential propagation in the nerve, resulted in no neural activity recorded, confirming the neural source of the pre-lidocaine CAPs.

With regards to the microfluidics, three separate designs were tested to ensure channel integrity during device deformation in [1]. Design 1 consisted of standard channel dimensions (20 μm H $\times$ 250 μm W), design 2 incorporated mid-channel supporting walls (20 μm H $\times$ 20 μm W $\times$ 390 μm L), and design 3 incorporated channel sections of narrower width and lower aspect ratio (150 μm and 250 μm W). Fluidic characterization of designs 1 and 3 showed that in the curled configuration, flow was achieved in 3 out of 4 microfluidic channels. Flow through some channels was blocked by pinching of the horizontal feeder channel as previously described. Design 2 maintained channel integrity during deformation and successfully achieved flow through all channels and outlet ports at various flow rates (nL/min to μL/min). Design 2 was selected for all animal testing.

The fluidic connection proved to be flexible, robust, and leak-free up to 2500 nL/min flow rates. Pressure measurements were collected for various flow rate settings programmed into the syringe pump. No leakage or delamination was observed when infusing the LACE microfluidic channels up to a mean pressure of 0.39 psi (2.69 kPa). The mean failure pressure value determined is an estimation and not necessarily the true value of the pressure at the device level. This value is useful as a point of reference for *in vivo* studies where a pressure driven fluidic flow system is utilized. Localized fluid delivery on a nerve phantom was demonstrated at low flow rates. Successful fluid flow through all channels and localized drug delivery are important for targeting multiple fascicles within the nerve and achieve high selectivity.

Acute *in vivo* infusion tests demonstrated that the LACE device can provide localized drug delivery to sciatic nerve fascicles. After implantation, some non-functioning ports became functional indicating that the implant procedure might have dislodged air bubbles from some channels. In some cases, only one or two ports seemed functional suggesting that device handling with surgical forceps could have caused other channels to become occluded. The suture locking technique has been implemented in recent *in vivo* implantations resulting in minimized device handling and damage. The LACE can safely handle a flow rate of up to 250 nL/min when curled around a rat sciatic nerve, which greatly exceeds the typical epineurial space drug delivery rate of 17 nL/min. The LACE delivered up to 12 μL volume with no leakage or delamination observed in the *in vivo* flow experiments. Lysing agent infusion experiments are currently underway to determine the appropriate flow rate and infusion duration. If long infusions are required, lower flow rates ($\sim$17 nL/min) might be suitable, but if short infusions are adequate, then fast flow rates ($\sim$250 nL/min) may prove useful. The latter flow regimen succesfully achieved localized dye diffusion into the smallest fascicles of the nerve suggesting that the application of lysing agents and growth factors at this flow rate and duration could induce somewhat selective sprouting from small (sensory) fascicles, potentially giving the LACE higher selectivity.

VII. Conclusion

A Parylene peripheral nerve interface with integrated microfluidics for improved *in vivo* stability was designed, fabricated, characterized, and implemented *in vivo*. A fabrication process with low variability and high yield was developed using standard Parylene surface micromachining techniques. A novel interlocking mechanism facilitated placement of the LACE around rat sciatic nerves and provided adequate holding strength and fit around nerves with various diameters. Electrochemical characterization of the cuff electrodes demonstrated desirable properties for stimulation and recording of neural tissue. The acute *in vivo* neural recording experiment demonstrated the capability of the LACE to successfully record A-fiber CAPs from a rat sciatic nerve. Flow through all microfluidic channels and localized fluid delivery on a nerve phantom was achieved at $<\mu$L/min flow rates which will allow targeting of multiple fascicles within the nerve. Infusion experiments *in vivo* demonstrated that the LACE device can provide localized drug delivery to sciatic nerve fascicles. The targeted drug delivery achieved by the LACE in *in vivo* studies shows the potential of the device to induce selective sprouting from multiple nerve fascicles resulting in higher device selectivity.

Current work includes incorporation of Parylene treatments in LACE devices to improve insulation integrity and prolong the device *in vivo* performance. Both LACE recording and stimulation will be demonstrated in acute ($\sim$1 day) and chronic ($\sim$2 weeks) *in vivo* studies. The LACE *in vivo* dosing and administration regimen of lysing agents and neurotrophic factors will also be investigated to achieve axonal sprouting.

Acknowledgment

The authors would like to thank Barbara Boyajian for her help with characterization and testing. They would also like to thank Dr. Donghai Zhu and the members of the USC Biomedical Microsystems Laboratory for their assistance with this project.

REFERENCES

[1] A. M. Cobo, B. Boyajian, C. Larson, K. Schotten, V. Pikov, and E. Meng, "A parylene cuff electrode for peripheral nerve recording and drug delivery," in *Proc. IEEE 30th Int. Conf. Micro Electro Mech. Syst. (MEMS)*, Jan. 2017, pp. 506–509.

[2] A. E. Schultz and T. A. Kuiken, "Neural interfaces for control of upper limb prostheses: The state of the art and future possibilities," *PM R*, vol. 3, no. 1, pp. 55–67, 2011.

[3] M. R. Popovic, D. B. Popovic, and T. Keller, "Neuroprostheses for grasping," *Neurol. Res.*, vol. 24, no. 5, pp. 443–452, 2013.

[4] X. Navarro, T. B. Krueger, N. Lago, S. Micera, T. Stieglitz, and P. Dario, "A critical review of interfaces with the peripheral nervous system for the control of neuroprostheses and hybrid bionic systems," *J. Peripheral Nervous Syst.*, vol. 10, no. 3, pp. 229–258, 2005.

[5] J. Wright, V. G. Macefield, A. van Schaik, and J. C. Tapson, "A review of control strategies in closed-loop neuroprosthetic systems," *Frontiers Neurosci.*, vol. 10, p. 312, Jul. 2016.

[6] N. G. Hatsopoulos and J. P. Donoghue, "The science of neural interface systems," *Annu. Rev. Neurosci.*, vol. 32, pp. 249–266, Jul. 2009.

[7] M. A. Lebedev and M. A. L. Nicolelis, "Brain-machine interfaces: Past, present and future," *Trends Neurosci.*, vol. 29, no. 9, pp. 536–546, 2006.

[8] T. Stieglitz, M. Schuetter, and K. P. Koch, "Implantable biomedical microsystems for neural prostheses," *IEEE Eng. Med. Biol. Mag.*, vol. 24, no. 5, pp. 58–65, Sep. 2005.

[9] S. Micera, M. C. Carrozza, L. Beccai, F. Vecchi, and P. Dario, "Hybrid bionic systems for the replacement of hand function," *Proc. IEEE*, vol. 94, no. 9, pp. 1752–1762, Sep. 2006.

[10] P. M. Rossini *et al.*, "Double nerve intraneural interface implant on a human amputee for robotic hand control," *Clin. Neurophysiol.*, vol. 121, no. 5, pp. 777–783, 2010.

[11] A. Branner, R. B. Stein, and R. A. Normann, "Selective stimulation of cat sciatic nerve using an array of varying-length microelectrodes," *J. Neurophysiol.*, vol. 85, pp. 1585–1594, Apr. 2001.

[12] G. G. Naples, J. T. Mortimer, A. Scheiner, and J. D. Sweeney, "A spiral nerve cuff electrode for peripheral nerve stimulation," *IEEE Trans. Biomed. Eng.*, vol. BME-35, no. 11, pp. 905–916, Nov. 1988.

[13] F. J. Rodríguez *et al.*, "Polyimide cuff electrodes for peripheral nerve stimulation," *J. Neurosci. Methods*, vol. 98, no. 2, pp. 105–118, 2000.

[14] G. E. Loeb and R. A. Peck, "Cuff electrodes for chronic stimulation and recording of peripheral nerve activity," *J. Neurosci. Methods*, vol. 64, pp. 95–103, Jan. 1996.

[15] J. T. Mortimer and N. Bhadra, "Peripheral nerve and muscle stimulation," in *Neuroprosthetics: Theory and Practice*. Singapore: World Scientific, 2004, pp. 638–682.

[16] X. Kang, J. Q. Liu, H. Tian, B. Yang, Y. Nuli, and C. Yang, "Self-closed parylene cuff electrode for peripheral nerve recording," *J. Microelectromech. Syst.*, vol. 24, no. 2, pp. 319–332, Apr. 2015.

[17] D. W. Tan, M. A. Schiefer, M. W. Keith, J. R. Anderson, J. Tyler, and D. J. Tyler, "A neural interface provides long-term stable natural touch perception," *Sci. Transl. Med.*, vol. 6, no. 257, pp. 138–257, 2014.

[18] B. P. Christie *et al.*, "Long-term stability of stimulating spiral nerve cuff electrodes on human peripheral nerves," *J. Neuroeng. Rehabil.*, vol. 14, p. 70, Jul. 2017.

[19] D. J. Tyler and D. M. Durand, "Functionally selective peripheral nerve stimulation with a flat interface nerve electrode," *IEEE Trans. Neural Syst. Rehabil. Eng.*, vol. 10, no. 4, pp. 294–303, Dec. 2002.

[20] C. Krarup, G. E. Loeb, and G. H. Pezeshkpour, "Conduction studies in peripheral cat nerve using implanted electrodes: II. The effects of prolonged constriction on regeneration of crushed nerve fibers," *Muscle Nerve*, vol. 11, no. 9, pp. 933–944, 1988.

[21] J. O. Larsen, M. Thomsen, M. Haugland, and T. Sinkjær, "Degeneration and regeneration in rabbit peripheral nerve with long-term nerve cuff electrode implant: A stereological study of myelinated and unmyelinated axons," *Acta Neuropathol.*, vol. 96, pp. 365–378, Oct. 1998.

[22] T. Suzuki, N. Kotake, K. Mabuchi, and S. Takeuchi, "Flexible regeneration-type nerve electrode with integrated microfluidic channels," in *Proc. Int. Conf. Microtechnol. Med. Biol.*, 2006, pp. 303–305.

[23] T. Stieglitz, H. Beutel, and J.-U. Meyer, "A flexible, light-weight multichannel sieve electrode with integrated cables for interfacing regenerating peripheral nerves," *Sens. Actuators A, Phys.*, vol. 60, pp. 240–243, May 1997.

[24] N. Lago, K. Yoshida, K. P. Koch, and X. Navarro, "Assessment of biocompatibility of chronically implanted polyimide and platinum intrafascicular electrodes," *IEEE Trans. Biomed. Eng.*, vol. 54, no. 2, pp. 281–290, Feb. 2007.

[25] M. Frankel, "Peripheral nerve interface, intraneural electrode," in *Encyclopedia of Computational Neuroscience*. New York, NY, USA: Springer-Verlag, 2015, pp. 2297–2299.

[26] T. Boretius *et al.*, "A transverse intrafascicular multichannel electrode (TIME) to interface with the peripheral nerve," *Biosensors Bioelectron.*, vol. 26, no. 1, pp. 62–69, 2010.

[27] A. Branner and R. A. Normann, "A multielectrode array for intrafascicular recording and stimulation in sciatic nerve of cats," *Brain Res. Bull.*, vol. 51, pp. 293–306, 2000.

[28] S. M. Lawrence, G. S. Dhillon, and K. W. Horch, "Fabrication and characteristics of an implantable, polymer-based, intrafascicular electrode," *J. Neurosci. Methods*, vol. 131, pp. 9–26, Dec. 2003.

[29] J. J. FitzGerald, S. P. Lacour, S. B. McMahon, and J. W. Fawcett, "Microchannels as axonal amplifiers," *IEEE Trans. Biomed. Eng.*, vol. 55, no. 3, pp. 1136–1146, Mar. 2008.

[30] A. F. Mensinger *et al.*, "Chronic recording of regenerating VIIIth nerve axons with a sieve electrode," *J. Neurophysiol.*, vol. 83, no. 1, pp. 611–615, 2000.

[31] J. Badia, T. Boretius, A. Pascual-Font, E. Udina, T. Stieglitz, and X. Navarro, "Biocompatibility of chronically implanted transverse intrafascicular multichannel electrode (TIME) in the rat sciatic nerve," *IEEE Trans. Biomed. Eng.*, vol. 58, no. 8, pp. 2324–2332, Apr. 2011.

[32] T. Lefurge, E. Goodall, K. Horch, L. Stensaas, and A. Schoenberg, "Chronically implanted intrafascicular recording electrodes," *Ann. Biomed. Eng.*, vol. 19, no. 2, pp. 197–207, 1991.

[33] S. M. Lawrence, J. O. Larsen, K. W. Horch, R. Riso, and T. Sinkjær, "Long-term biocompatibility of implanted polymer-based intrafascicular electrodes," *J. Biomed. Mater. Res.*, vol. 63, no. 5, pp. 501–506, 2002.

[34] F. Viterbo, J. C. Trindade, K. Hoshino, and A. Mazzoni, "Two end-to-side neurorrhaphies and nerve graft with removal of the epineural sheath: Experimental study in rats," *Brit. J. Plastic Surg.*, vol. 47, pp. 75–80, Jan. 1994.

[35] P. Tos, G. Colzani, D. Ciclamini, P. Titolo, P. Pugliese, and S. Artiaco, "Clinical applications of end-to-side neurorrhaphy: An update," *BioMed Res. Int.*, vol. 2014, Jul. 2014, Art. no. 646128.

[36] F. Šámal, P. Haninec, O. Raška, and P. Dubový, "Quantitative assessment of the ability of collateral sprouting of the motor and primary sensory neurons after the end-to-side neurorrhaphy of the rat musculocutaneous nerve with the ulnar nerve," *Ann. Anatomy-Anatomischer Anzeiger*, vol. 188, pp. 337–344, Jul. 2006.

[37] U. Kovačič, T. Tomšič, T. Žele, J. Sketelj, and F. F. Bajrović, "Influence of breaching the connective sheaths of the donor nerve on its myelinated sensory axons and on their sprouting into the end-to-side coapted nerve in the rat," *J. Neurotrauma*, vol. 29, no. 8, pp. 2805–2815, 2012.

[38] P. Haninec, R. Kaiser, and P. Dubový, "A comparison of collateral sprouting of sensory and motor axons after end-to-side neurorrhaphy with and without the perineurial window," *Plastic Reconstructive Surg.*, vol. 130, no. 3, pp. 609–614, 2012.

[39] H.-F. Liu, Z.-G. Chen, T.-L. Fang, P. Arnold, W. C. Lineaweaver, and J. Zhang, "Changes of the donor nerve in end-to-side neurorrhaphies with epineurial window and partial neurectomy: A long-term evaluation in the rat model," *Microsurgery*, vol. 34, no. 2, pp. 136–144, 2014.

[40] B. Rydevik, M. D. Brown, T. Ehira, and C. Nordborg, "Effects of collagenase on nerve tissue. An experimental study on acute and long-term effects in rabbits," *Spine*, vol. 10, pp. 562–566, Jul./Aug. 1985.

[41] W. V. McCallister, P. Tang, J. Smith, and T. E. Trumble, "Axonal regeneration stimulated by the combination of nerve growth factor and ciliary neurotrophic factor in an end-to-side model," *J. Hand Surg. Amer.*, vol. 26, pp. 478–488, May 2001.

[42] W.-C. Liao, Y.-J. Wang, M.-C. Huang, and G.-F. Tseng, "Methylcobalamin facilitates collateral sprouting of donor axons and innervation of recipient muscle in end-to-side neurorrhaphy in rats," *PLoS ONE*, vol. 8, no. 9, p. e76302, 2013.

[43] L. G. Isaacson, B. N. Saffran, and K. A. Crutcher, "Nerve growth factor-induced sprouting of mature, uninjured sympathetic axons," *J. Comparative Neurol.*, vol. 326, no. 3, pp. 327–336, 1992.

[44] W.-C. Liao, Y.-J. Wang, M.-C. Huang, and G.-F. Tseng, "Methylcobalamin facilitates collateral sprouting of donor axons and innervation of recipient muscle in end-to-side neurorrhaphy in rats," *PLoS ONE*, vol. 8, no. 9, p. e76302, 2013.

[45] K. M. Rich, J. R. Luszczynski, P. A. Osborne, and E. M. Johnson, Jr., "Nerve growth factor protects adult sensory neurons from cell death and atrophy caused by nerve injury," *J. Neurocytol.*, vol. 16, pp. 261–268, Apr. 1987.

[46] A. Cobo, K. Scholten, J. Yoo, T. Hudson, V. Pikov, and E. Meng, "A parylene peripheral nerve cuff electrode with integrated microfluidics," in *Proc. 17th Conf. Solid-State Sens., Actuators Microsyst.*, Hilton Head, SC, USA, 2016, pp. 1–4.

[47] E. Meng, *Biomedical Microsystems*. Boca Raton, FL, USA: CRC Press, 2011.

[48] B. J. Kim and E. Meng, "Micromachining of Parylene C for bioMEMS," *Polym. Adv. Technol.*, vol. 27, no. 5, pp. 564–576, 2015.

[49] H. Schmalbruch, "Fiber composition of the rat sciatic nerve," *Anatom. Rec.*, vol. 215, no. 1, pp. 71–81, 1986.

[50] C. H. Mastrangelo and G. S. Saloka, "A dry-release method based on polymer columns for microstructure fabrication," in *Proc. IEEE Invest. Micro Struct., Sens., Actuators, Mach. Syst. Micro Electro Mech. Syst. (MEMS)*, Feb. 1993, pp. 77–81.

[51] T.-J. Yao, X. Yang, and Y.-C. Tai, "BrF_3 dry release technology for large freestanding parylene microstructures and electrostatic actuators," *Sens. Actuators A, Phys.*, vols. 97–98, pp. 771–775, Apr. 2002.

[52] B. Wang, A. Petrossians, and J. D. Weiland, "Reduction of edge effect on disk electrodes by optimized current waveform," *IEEE Trans. Biomed. Eng.*, vol. 61, pp. 2254–2263, 2014.

[53] J. S. Ordonez *et al.*, "Cuff electrodes for very small diameter nerves—Prototyping and first recordings *in vivo*," in *Proc. 36th Annu. Int. Conf. IEEE Eng. Med. Biol. Soc. (EMBC)*, Aug. 2014, pp. 6846–6849.

[54] H. Yu, W. Xiong, H. Zhang, W. Wang, and Z. Li, "A parylene self-locking cuff electrode for peripheral nerve stimulation and recording," *J. Micoelectromech. Syst.*, vol. 23, no. 5, pp. 1025–1035, Oct. 2014.

[55] N. Xue *et al.*, "Polymeric C-shaped cuff electrode for recording of peripheral nerve signal," *Sens. Actuators B, Chem.*, vol. 210, pp. 640–648, Apr. 2015.

[56] L. A. Geddes and R. Roeder, "Criteria for the selection of materials for implanted electrodes," *Ann. Biomed. Eng.*, vol. 31, no. 7, pp. 879–890, 2003.

[57] Y. Nam, "Material considerations for *in vitro* neural interface technology," *MRS Bull.*, vol. 37, pp. 566–572, Jun. 2012.

[58] A. Cowley, "A healthy future: Platinum in medical applications," *Platinum Metals Rev.*, vol. 55, no. 2, pp. 98–107, 2011.

[59] B. Kim, B. Chen, M. Gupta, and E. Meng, "Formation of three-dimensional Parylene C structures via thermoforming," *J. Micromech. Microeng.*, vol. 24, no. 6, p. 065003, 2014.

[60] M.-S. Ju, C.-C. K. Lin, J.-L. Fan, and R.-J. Chen, "Transverse elasticity and blood perfusion of sciatic nerves under *in situ* circular compression," *J. Biomech.*, vol. 39, no. 1, pp. 97–102, 2006.

[61] V. Normand, D. L. Lootens, E. Amici, K. P. Plucknett, and P. Aymard, "New insight into agarose gel mechanical properties," *Biomacromolecules*, vol. 1, no. 4, pp. 730–738, 2000.

[62] D. Zhan, J. Velmurugan, and M. V. Mirkin, "Adsorption/desorption of hydrogen on Pt nanoelectrodes: Evidence of surface diffusion and spillover," *J. Amer. Chem. Soc.*, vol. 131, no. 41, pp. 14756–14760, 2009.

[63] S. F. Cogan, "Neural stimulation and recording electrodes," *Annu. Rev. Biomed. Eng.*, vol. 10, pp. 275–309, Aug. 2008.

[64] E. A. Pohlmeyer, L. R. Jordon, P. Kim, and L. E. Miller, "A fully implanted drug delivery system for peripheral nerve blocks in behaving animals," *J. Neurosci. Methods*, vol. 182, no. 2, pp. 165–171, 2009.

[65] G. Cirillo *et al.*, "Reactive astrocytosis-induced perturbation of synaptic homeostasis is restored by nerve growth factor," *Neurobiol. Disease*, vol. 41, no. 3, pp. 630–639, 2011.

[66] H. Herken and F. Hucho, *Selective Neurotoxicity*. Berlin, Germany: Springer, 2012.

Angelica M. Cobo received the B.S. degree in biomedical engineering from Florida International University in 2008 and the M.S. degree in biomedical engineering from the University of Southern California in 2012, where she is currently pursuing the Ph.D. degree in biomedical engineering with a focus on the development of implantable polymer-based MEMS devices, such as a peripheral nerve cuff electrode for restoration of sensorimotor function in amputees and a wireless drug delivery device for management of chronic diseases, and rare childhood cancers. She was a Research Assistant with the Bioengineering Laboratory, Diabetes Research Institute, where she focused on the development of a bioactive scaffold material for use in cellular replacement therapies to treat Type 1 Diabetes Mellitus. She was a recipient of the Viterbi School of Engineering Ph.D. Merit Fellowship, the Women in Science and Engineering Merit Award, and the Alfred E. Mann Institute Biomedical Engineering Doctoral Fellowship.

Christopher E. Larson received the bachelor's degree in music composition from Biola University, CA, USA, in 2009, and the B.S. degree in biomedical engineering from the University of Southern California in 2015, where he is currently pursuing the Ph.D. degree with the Biomedical Microsystems Laboratory, developing implantable medical devices based on microelectromechanical systems. His current focus is neural interfaces with integrated drug delivery capabilities.

Kee Scholten received the B.S. degree in applied physics from the California Institute of Technology in 2009 and the Ph.D. degree in applied physics from the University of Michigan under Prof. E. Zellers in 2014, with a research focus on gas-phase microsensors for environmental monitoring and biomedical diagnostics. He is currently a Post-Doctoral Scholar with the Biomedical Microsystems Laboratory, University of Southern California. His current and on-going work entails the development of implantable microsensors for use in biomedical applications. His research explores the development of micro- and nano-technology for ubiquitous chemical and biomedical sensing, with a focus on microelectromechanical systems, including microfluidic transducers for chemical sensing and flexible electrochemical interfaces for neural-machine interfaces.

Jason A. Miranda received the B.S. degree in cell biology and physiology from Arizona State University and the Ph.D. degree in neuroscience from The University of Texas at Austin. He received a Post-Doctoral Fellowship from Emory University, all studying the role of reproductive hormones in animal behavior, auditory processing, and neuroplasticity. From 2009 to 2016, he worked to develop treatments for cognitive and sensory disorders at Pfizer Ltd. He is currently an Investigator at Galvani Bioelectronics, where he evaluates and develops new technologies to treat chronic disease through peripheral nerve stimulation and recording.

Sahar Elyahoodayan received the B.S. degree in biomedical engineering, the M.S. degree in biomedical engineering, and the M.S. degree in electrical engineering from the University of Southern California in 2013, 2013, and 2017, respectively, where she is currently pursuing the Ph.D. degree with the Center for Neural Engineering. She was a Research Assistant with the Biomedical Microsystems Laboratory, where she was involved in a wireless drug delivery pump for use in chronic patients with chronic conditions. Her research interests are electrophysiology, drug delivery, animal experiments, and neuro-modulation system design.

Dong Song (S'02–M'04) received the B.S. degree in biophysics from the University of Science and Technology of China in 1994 and the Ph.D. degree in biomedical engineering from the University of Southern California in 2004. He is currently a Research Associate Professor with the Department of Biomedical Engineering, University of Southern California. His research interests include computational modeling of the nervous system, hippocampal memory prostheses, and neural interface technology. He was a recipient of the Society for Brain Mapping and Therapeutics Young Investigator Award. He is a member of American Statistical Association, the Biomedical Engineering Society, IEEE, the Society for Brain Mapping and Therapeutics, and the Society for Neuroscience.

Victor Pikov received the B.S. degree in biopsychology from the Vassar College in 1995 and the Ph.D. degree in cell biology and neuroscience from Georgetown University in 2000. He competed the post-doctoral training in molecular neuroscience at the California Institute of Technology in 2002. From 2002 to 2015, he performed preclinical neural engineering research at the Huntington Medical Research Institutes. Since 2015, he has been the Director of Research Platforms and Tools at the GlaxoSmithKline Bioelectronics Division, which, in 2016, emerged as an independent company Galvani Bioelectronics. Since 2018, he has been a CEO of Medipace Inc., working on development of implantable stimulation-based therapies for the GI tract. His research interests include the development of advanced implantable neuromodulation devices and nerve cuff interfaces and their clinical application for chronic illnesses, such as autoimmune, metabolic, urologic, and reproductive diseases.

Ellis Meng (M'02–SM'09–F'16) received the B.S. degree in engineering and applied science and the M.S. and Ph.D. degrees in electrical engineering from the California Institute of Technology, Pasadena, in 1997, 1998, and 2003, respectively. Since 2004, she has been with the University of Southern California, Los Angeles, where she is currently a Professor of biomedical engineering. She was previously the Dwight C. and Hildagarde E. Baum Chair of the Department of Biomedical Engineering from 2015 to 2018. She held the Viterbi Early Career Chair at the Viterbi School of Engineering and is currently an inaugural holder of a Gabilan Distinguished Professorship in science and engineering. She also holds a joint appointment at the Ming Hsieh Department of Electrical Engineering. Her research interests include bio-MEMS, implantable biomedical microdevices, microfluidics, multimodality integrated microsystems, and packaging. She is a member of Tau Beta Pi, the Biomedical Engineering Society, the American Institute for Medical and Biological Engineering, the American Society of Mechanical Engineers, and the American Society for Engineering Education. She is a fellow of ASME, BMES, and AIMBE. Her honors include the NSF CAREER Award, the Wallace H. Coulter Foundation Early Career Award, the 2009 TR35 Young Innovator Under 35, the Viterbi Early Career Chair, the ASEE Curtis W. McGraw Research Award, and the 2018 IEEE Engineering in Medicine and Biology Society Technical Achievement Award.